

PCCP

Accepted Manuscript



This is an *Accepted Manuscript*, which has been through the Royal Society of Chemistry peer review process and has been accepted for publication.

Accepted Manuscripts are published online shortly after acceptance, before technical editing, formatting and proof reading. Using this free service, authors can make their results available to the community, in citable form, before we publish the edited article. We will replace this *Accepted Manuscript* with the edited and formatted *Advance Article* as soon as it is available.

You can find more information about *Accepted Manuscripts* in the [Information for Authors](#).

Please note that technical editing may introduce minor changes to the text and/or graphics, which may alter content. The journal's standard [Terms & Conditions](#) and the [Ethical guidelines](#) still apply. In no event shall the Royal Society of Chemistry be held responsible for any errors or omissions in this *Accepted Manuscript* or any consequences arising from the use of any information it contains.



Physical Chemistry Chemical Physics

ARTICLE

First Principles Modeling of Mo₆S₉ Nanowire *via* Condensation of Mo₄S₆ Clusters and Effect of Iodine Doping on Structural and Electronic Properties

Received 00th January 20xx,
Accepted 00th January 20xx

DOI: 10.1039/x0xx00000x

www.rsc.org/

Iflah Laraib,^a† J. Karthikeyan,^{a,b}† P. Murugan^{a,b*}

By employing first principles DFT calculations, we propose new stable model for Mo₆S₉ nanowire (NW) obtained by condensing tetrahedral Mo₄S₆ clusters rather than octahedral Mo₆S₈ clusters, which are known as magic clusters in Mo-S polyhedral cluster family. The pristine NW is found to be metallic and its local structure and physical properties can be tuned by doping of iodine atoms. This doping increases the number of Mo-Mo bonds in the NW, thus, Mo₄ tetrahedra are initially fused to Mo₆ octahedron, and then, to Mo₈ dodecahedron. Further, a close correlation among the Mo-Mo bonding in the local structure, mechanical and electronic properties is observed from our study. Finally, the stability of the pristine and iodine doped Mo₆S_{9-x}I_x NW structures obtained from condensation of Mo₄ tetrahedra, are found to be quite comparable with that of already reported Mo₆S_{9-x}I_x NWs with Mo₆ octahedra as building blocks.

Introduction

In recent years, Mo-S based nanostructured compounds have been studied due to their interesting properties such as tunable electronic and magnetic behaviour¹⁻⁴, high tensile strength⁵⁻⁷, and unique optical response^{8,9}. These properties pave the way for obtaining nanostructures with various dimensions that find potential applications in fabricating compact and efficient nano-electronic, optoelectronic, photovoltaic⁹⁻¹¹, and energy storage devices^{6, 12-14}. Among them, single layer of 2H-MoS₂ nanosheet besides being semiconducting in nature, with a direct band gap of 1.8 eV¹⁵, exhibits valley polarization^{16,17}. While the 1-D Mo-S compounds, such as sub-nano meter sized Mo₆S₉ and Mo₆S₆ nanowires (NWs), have tunable electronic, magnetic, and mechanical properties that can be achieved by either addition of Li or doping of iodine atoms¹⁸⁻²². Also, they were proposed to be useful in developing new molecular sensors^{10, 23-25}, interconnects^{26,27} and switches²⁸, and low dimensional superconductors²⁹ and energy storage devices³⁰. Interestingly, 0-D MoS_{2+x} planar clusters that have good catalytic properties³¹ towards hydrogen evolution reaction³² and hydro desulfurization, were formed in different geometries^{22,23} on various substrates like Au, graphite, TiO₂ and graphene³³.

Additionally, it was also reported³⁴⁻³⁶ that Mo₄S₆ and Mo₆S₈ clusters are stable among small sized Mo_xS_y polyhedral

clusters. Particularly, the Mo₄S₆ and Mo₆S₈ clusters are found to have ultrahigh stability as they possess high structural symmetry and large highest occupied molecular orbital – lowest unoccupied molecular orbital (HOMO-LUMO) gap.^{28,29} Structurally, Mo₆S₈ cluster consists of a Mo₆ octahedral core with eight S atoms capped on its faces. Its highly symmetric structure and the nature of orbitals provide it a tendency to condense into one dimensional structures such as Mo₆S_{9-y}I_y and Mo₆S_{6-y}I_y NWs.³⁰ The proposed structure from the atomic pair distribution function (PDF) analysis of powder X-ray diffraction data³⁷ show that the skeleton of the former NW is Mo₆ octahedra which is decorated with six S/I atoms on its faces and three S/I atoms on the bridging sites in between the octahedral.^{22, 26} In another report,¹⁹ the pristine form of this NW has been condensed by alternate stacking of Mo₆S₆ octahedron and two Mo₃S₃ triangles that are interconnected by addition of three S atoms. However, this NW was reproducibly synthesized only for a certain range of doping of I atom (i.e, $y = 4.5$ to 6.0). It was also observed by first principles calculations that shortage of I atoms leads to deformation of the Mo₆ octahedra into Mo₃ triangles or prism, due to insufficient electrons to form Mo-Mo network.¹⁹ On the other hand, Mo₄S₆ cluster consists of a Mo₄ tetrahedron with six S atoms capped on its edges²⁸ and a larger HOMO-LUMO gap of ≈ 1.57 eV as compared to that of Mo₆S₈ cluster (= 0.91 eV).²⁹ The studies using density functional theory (DFT)^{38,39} and Auger spectroscopy⁴⁰ on this cluster deposited on metallic surfaces have been carried out to understand their thermal and chemical properties. Till date, there is no report on condensation of Mo₄S₆ cluster. Indeed, it is one of the ways to derive new nanostructures. In the present study, we show, by employing first principle density functional calculations that two Mo₄S₆ clusters prefer to

^a Functional Materials Division, CSIR – Central Electrochemical Research Institute, Karaikudi–630 003, Tamil Nadu, India.

^b Academy of Scientific and Innovative Research, CSIR – Central Electrochemical Research Institute, Karaikudi–630 003, Tamil Nadu, India.

† These authors have equally contributed in this work.

Electronic Supplementary Information (ESI) available: [1] Optimized structures of (Mo₄S₆)_n finite nanorods. 2) E_c and E_{HOMO-LUMO} of (Mo₆S₁₂)_n finite nanorods. 3) The ball and stick models of optimized the 1-D and 2-D Mo₆S₁₂ assemblies, and 4) their energetics, 5) Optimized structure of Mo₆S₁₂ NW, and 6) Plot of total energy per atom (E) vs. lattice parameter (c) for Mo₆S₁₂ and Mo₆S₉ NWs.]. See DOI: 10.1039/x0xx00000x

ARTICLE

condense linearly as similar to fusion of octahedral clusters. Then, the condensation is extended for understanding the structural stability and electronic properties of $(\text{Mo}_4\text{S}_6)_n$ nanorods with $n = 1$ to 8 as well as NWs. Interestingly, our calculations reveal that pristine Mo_8S_{12} NW, obtained from condensation of Mo_4S_6 clusters, is energetically more stable as compared to the existing model of Mo_6S_9 NW which was reported.³² Although, $\text{Mo}_8\text{S}_{12-x}\text{I}_x$ NWs with $x = 2 - 8$ are found to be less stable, both the NWs with $x = 10$ have almost equal structural stability. Further, the structural, mechanical, and electronic properties of the Mo_8S_{12} NW are tuned by varying the local structure of Mo clusters *via* I atom doping.

Computational Methods

The atomic structure of Mo-S clusters and NWs are self-consistently optimized using first principles DFT calculations as implemented by Vienna *Ab initio* Simulation Package (VASP)⁴¹. The wave functions are expanded using plane wave basis set within projector augmented wave pseudo-potential formalism⁴² and electron-electron correlation effects are corrected by generalized gradient approximations⁴³, invoking GGA (Perdew-Wang 91) functional. The electronic optimizations are carried out with convergence factor of 10^{-6} eV and then, the ions are relaxed iteratively until the absolute values of forces between the ions become less than 0.01 eV/Å. The Mo-S cluster is kept in a periodic unit-cell with a vacuum space of 15 Å in all directions, which is necessary to avoid the interactions between the cluster and its periodic images. Similarly, $\text{Mo}_8\text{S}_{12-x}\text{I}_x$ NWs are oriented along z-axis of the unit-cell, in which, both x and y directions are considered to have a vacuum space of 15 Å. Then, the lattice constant of the NW is manually optimized by varying steps of 0.01 Å. To deduce the DOS and band structure, the non-self-consistent calculations are performed, in which makes use of the charge density and wave functions that are previously obtained from self-consistent calculations. For self-consistent and non-self-consistent calculations, the Brillouin zone of the simulation cell is sampled by $1 \times 1 \times 6$ and $1 \times 1 \times 200$ k-meshes, respectively. To find the magnetic properties of the NWs, the spin-polarized calculations were carried out. Our study confirmed that all the NWs were observed to be non-magnetic, because Mo atoms are firmly bonded as well as I atoms are symmetrically distributed in NWs^{2,29}. For comparing the stability of $\text{Mo}_8\text{S}_{12-x}\text{I}_x$ NWs, similar calculations were repeated for $\text{Mo}_6\text{S}_9\text{I}_y$ NWs whose atomic structures were reported³².

Results and discussion

Initially Mo_4S_6 cluster is modeled by edge-capping S atoms on a Mo_4 tetrahedron (refer Figure 1) and this cluster is optimized by first principles calculations. It has HOMO-LUMO gap of 1.57 eV which is in agreement with earlier works^{28,29}. Note that the average Mo-Mo and Mo-S bond lengths in the cluster are 2.56 and 2.32 Å, respectively. It is also observed

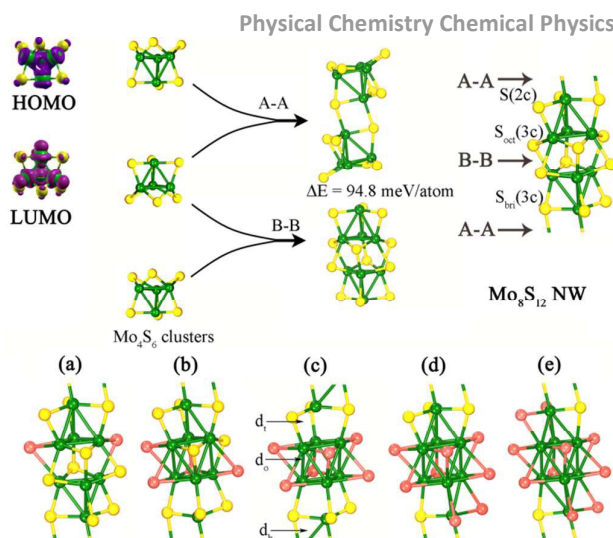


Figure 1. Top panel shows the HOMO and LUMO diagrams of Mo_4S_6 clusters and its condensation *via* A-A and B-B configurations, leading to infinite Mo_8S_{12} NW. In bottom panel, Figures (a – e) depict the optimized structure of $\text{Mo}_8\text{S}_{12-x}\text{I}_x$ NWs with $x = 2, 4, 6, 8$, and 10. Green, yellow and pink balls indicate Mo, S, and I atoms, respectively. Three different types of S labeled are represented as S(2c), $\text{S}_{\text{oct}}(3\text{c})$ and $\text{S}_{\text{brn}}(3\text{c})$ in Mo_8S_{12} NW, and different Mo-Mo bonding sites are labeled as d_v , d_v , d_o .

that the HOMO of the cluster is localized on S atoms while the LUMO lies mainly on Mo atoms (refer Figure 1). This indicates that the Mo atoms of one tetrahedron can interact with the S atoms present in another tetrahedron for making Mo-S bonds through sharing of electrons, when two Mo_4S_6 clusters are fused to form a dodecahedron cluster. In addition to that, the symmetry of HOMO and LUMO enables the clusters to condense together.

To begin with, two units of the Mo_4S_6 cluster can fuse into two possible ways: *viz.* A-A and B-B configurations (shown in Figure 1). In A-A configuration, two tetrahedra interact by forming two Mo-S bonds with their apexes pointing each other, while in the B-B, their triangular bases lie face to face, thereby forming six Mo-S bonds. Our calculations show that the B-B configuration is 2.22 eV more stable than the A-A counterpart due to having more Mo-S bonds. Therefore, we proceed with further condensation of Mo_4S_6 cluster onto B-B configuration, to obtain $(\text{Mo}_4\text{S}_6)_3$ cluster, in which, both A-A and B-B linkages are present because a third unit can be added only *via* A-A bridge. In similar fashion, $(\text{Mo}_4\text{S}_6)_n$ nano-rods with $n = 2 - 8$ are obtained and the optimized structures are shown in Figure S1 (Supplementary Information). To understand the stability of $(\text{Mo}_4\text{S}_6)_n$ nano-rods, the condensation energy per Mo_4S_6 formula unit (f.u.) is deduced from $E_{\text{cond}} = \frac{n \times \text{Mo}_4\text{S}_6 - (\text{Mo}_4\text{S}_6)_n}{n}$. The calculated E_{cond} value and the HOMO-LUMO gap of nanorods are reported in Figure S2 (Supplementary Information). It shows that the E_{cond} value increases gradually with n , whereas, the HOMO-LUMO gap decreases due to the creation of new electronic energy levels that originate from Mo-S bonds formed during condensation. Further, trend of this plot indicates that the Mo_4S_6 units are plausibly condensed to form the infinite Mo_8S_{12} NW, whose unit-cell contains two units connected alternatively through B-B and A-A linkages. We also performed the first principles calculations on 2-D assembly which is possible to construct only through A-A configuration, because of the geometrical

constraint in making Mo-S bond along x and y direction due to the presence of B-B linkage. The optimized structure and its energetics are reported in Figure S3 and S4 (Supplementary Information).

The atomic structure of Mo_8S_{12} NW is provided in Figure 1 and its lattice constant is calculated to be 9.91 Å. In this structure, average Mo-Mo and Mo-S bond lengths in the constituent Mo_4 tetrahedra are 2.75 Å and 2.32 Å, respectively. Note that the Mo-Mo bond length in isolated Mo_4S_6 cluster is 2.56 Å which is quite shorter than that in the NW, owing to the formation of more number of Mo-S bonds during the condensation of clusters. It is also observed that the Mo-S bond in A-A bridging site is larger by 0.2 Å as compared to that bond in B-B site. Further, we noticed that there is possibility to form Mo_6 octahedron in region where triangular bases of two Mo_4 units are interconnected with a Mo-Mo separation of 3.12 Å. In this region, the atomic structure of this NW is quite similar to Mo_6S_9 NW. Also we noticed that the Mo-Mo bond (= 2.60 Å) in the triangular base is quite shorter as compared to Mo-Mo bond along NW axis (2.75 Å). This suggests that the Mo_3 triangles will not break easily when the system undergoes structural changes due to the external causes such as, chemical doping or mechanical stress.³²

Next, we carried out the doping of I atoms into Mo_8S_{12} NW to understand its effect on the local atomic structure and electronic properties. For this, three different sulfur sites are identified in the NW, viz. $S_{\text{brf}}(3c)$, $S_{\text{oct}}(3c)$, and $S(2c)$ which are present at bridging, octahedral, and tetrahedral sites, respectively (shown in Figure 1) and 3c and 2c stand for three and two coordination of sulfur atom, respectively. Substitution of I atom in the aforesaid sites shows that it prefers to replace $S_{\text{oct}}(3c)$ atom, rather than $S_{\text{brf}}(3c)$ or $S(2c)$ atom. As compared to former site, doping of I atom on other two sites increases the ground state energy by 35.48 and 10.78 meV/f.u., respectively. Considering this, two $S_{\text{oct}}(3c)$ atoms are replaced with I atoms to get the $\text{Mo}_8\text{S}_{10}\text{I}_2$ NW. Our calculations on this NW show that the strength of Mo-Mo interaction at octahedral site is significantly increased as this distance is decreased to 3.02 Å from 3.12 Å (of pristine NW). On the contrary, same bond distances at tetrahedra as well as bridging sites are slightly increased, which is the symptom of formation of Mo_6 octahedron in $\text{Mo}_8\text{S}_{12-x}\text{I}_x$ NW with $x = 2$ (refer Figure 2). In the subsequent step of doping of two more I atoms ($x = 4$), the average Mo-Mo bond distances at octahedral (d_o) and bridging (d_b) sites are further decreased to 2.85 and 2.96 Å respectively, whereas, those at tetrahedra site (d_t) are increased from 2.81 Å (for $x = 2$ NW) to 2.96 Å. Hence, we conclude that the deformation of Mo_4 tetrahedra significantly starts from $x = 4$ onwards. With further doping of I atoms ($x = 6$), the Mo-Mo bond at d_o site almost reaches bulk Mo-Mo distance (=2.72 Å), which indicates that the NW has enough electrons to form a Mo_6 octahedron (Mo-Mo = 2.78 Å). Also the Mo-Mo bonds at d_b site get strengthened enough to maintain the A-A bridging bonds (Mo-Mo@ d_b = 2.91 Å). Hence, obviously the bonds at d_t become too weak to keep the Mo_4 tetrahedra intact anymore, as seen in Figures 1 and 2. From these discussions, we have clearly demonstrated that the

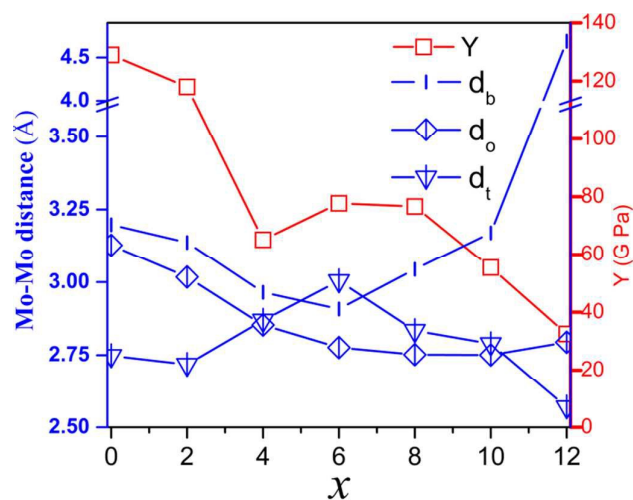


Figure 2. Young's modulus (Y) and average Mo-Mo distances at sites d_b , d_t and d_o for $\text{Mo}_8\text{S}_{12-x}\text{I}_x$ NWs against ' x '.

octahedral geometry is stable in iodine doped NWs while the tetrahedral geometry is preferred in pristine NWs.

Interestingly, we further discerned that the weakly interacting apex Mo atoms in $\text{Mo}_8\text{S}_6\text{I}_6$ NW are pulled back towards the Mo_6 octahedron when two more I atoms ($x = 8$) are substituted at $S(2c)$ sites (d_t) which was shown to be the next feasible site for doping of this atom. It is a trait of formation of Mo_8 dodecahedral unit which reduces the Mo-Mo bond lengths at d_t site (refer Figure 2). Thus, for the $\text{Mo}_8\text{S}_{12-x}\text{I}_x$ NW with $x = 8$, the Mo-Mo bond lengths at d_t decrease significantly, while those at d_b site increase to the same extent. The same trend is continued in the structure of NW when x is increased to 10. Finally, when all the S atoms are replaced with I atoms, the resulting atomic structure of Mo_8I_{12} NW is found to be broken into weakly interacting dodecahedron clusters with Mo-Mo bond distance of 4.69 Å at d_b site and the I-I distance of 4 Å (refer Figure S5, Supplementary Information). The larger radius of I atom as compared to S atom completely shields the Mo atom and prevents interaction between them. Note that Mo-Mo bond length in Mo_8 cluster is 2.56 Å, which is equal to corresponding distance in Mo_4S_6 isolated cluster. The above discussions show that the core Mo_4 tetrahedral structure of the pure NW first deforms into Mo_6 octahedron and later all the Mo atoms fuse into a Mo_8 dodecahedral cluster due to availability of sufficient number of electrons. Thus, we demonstrated that the local backbone geometry of Mo_n clusters in the NW network flexibly changes its structure from tetrahedra to octahedral one and then, finally to dodecahedral structure during the doping of I atoms.

To understand the stability of the NWs, the cohesive energy per atom (CE) and the formation energy per atom (FE) are calculated from the following formulae:

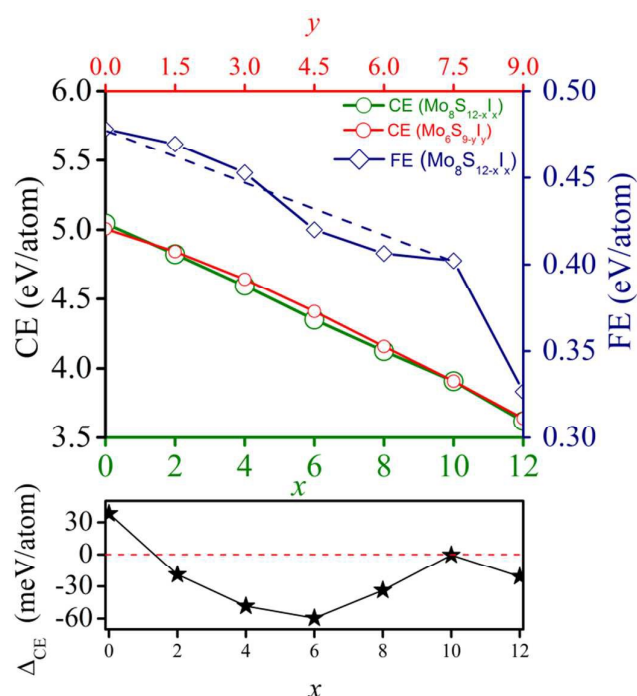


Figure 3. CE and FE of Mo₈S_{12-x}I_x and Mo₆S_{9-y}I_y NW against 'x' (bottom panel) and 'y' (top panel) respectively; along with $\Delta_{CE} = CE(Mo_8S_{12-x}I_x) - CE(Mo_6S_{9-y}I_y)$ against x.

For Mo₈S_{12-x}I_x NW,

$$CE = \frac{1}{20} [8 E(Mo) + (12 - x) E(S) + x E(I) - E(Mo_8S_{12-x}I_x)]$$

$$FE = \frac{1}{20} [8 \mu(Mo) + (12 - x) \mu(S) + x \mu(I) - E(Mo_8S_{12-x}I_x)]$$

where, E(Mo), E(S), E(I) and E(Mo₈S_{12-x}I_x) are the atomic energies of Mo, S, I atoms and total energy of Mo₈S_{12-x}I_x NW, respectively. It is worth to mention that all atomic energies are obtained by performing the spin-polarization calculations. While, $\mu(Mo)$, $\mu(S)$, and $\mu(I)$ are the chemical potentials of respective elements in their rich condition, thus they are obtained from bulk Mo, S₈ and I₂ clusters, respectively.^{38,39} Similar formulae are adopted for calculating the CE and FE of Mo₆S_{9-y}I_y NWs whose atomic structures were reported elsewhere³². Though the unit cells of Mo₆S_{9-x}I_x and Mo₈S_{12-x}I_x NWs contain different number of total atoms, the cohesive energy per atoms is calculated for both the NWs independently and then its difference (Δ_{CE}) is calculated between the nanowires for which $y = 3x/4$ that allows direct energy comparisons. For both types of NW, the CE value decreases gradually with increasing concentration of I atoms as a result of increasing ionic nature of NW (refer Figure 3). This figure reveals that the pristine Mo₈S₁₂ NW with tetrahedra as building blocks is found to be more stable than Mo₆S₉ NW,

Mo ₈ S _{12-x} I _x	Band gap (eV)	c (Å)	Y (GPa)	CE (eV/atom)	
				1-D	2-D
x = 0	metal	9.91	133	5.05	5.06
x = 2	metal	9.84	98.9	4.82	4.77
x = 4	0.15	9.89	87.4	4.60	4.48
x = 6	0.08	9.91	98	4.35	4.21
x = 8	0.29	9.74	95.3	4.12	3.96
x = 10	0.40	9.66	84.5	3.91	3.68
x = 12	0.89	10.75	41.3	3.62	3.38

Table 1. Band gap, Lattice Parameter (c), Young's modulus (Y) and Cohesive Energy (CE) of 1-D and 2-D Mo₈S_{12-x}I_x assemblies (x = 0 – 12).

by energy difference of 38.19 meV/atom (refer Figure S6, Supplementary Information). It is because of the fact that the building blocks of Mo₆S₉ NW (Mo₃ triangular clusters)³² have been found to be less stable than the magic tetrahedral and octahedral clusters.^{28, 29} Moreover, the I atom doped Mo₆S₉ NWs show the greater stability, because the atomic structure of Mo₈S_{12-x}I_x NW has one or two weakly bonded Mo_n cluster units. However, for x = 10, the CE values are almost equal for both the NWs due to formation of Mo₈ dodecahedron with more Mo-Mo bonds. Similarly, the FE is also decreased with increased concentration of I atoms. Initially, for the NWs with x = 2 and 4, the FE comes down gradually because of breaking of tetrahedral clusters but decreases very slowly after x = 6 due to formation of octahedral clusters in the structure. Finally the FE falls down to a minimum value for weakly interacting Mo₁₂I₁₂ dodecahedral clusters. The FE plot is linearly approximated¹⁸ (shown by dashed line in Figure 5) by connecting the FE of x = 0 and x = 10 case, to deduce the synthesizable composition of NWs. Note that the NW with x = 12 is not considered due to weakly interacting dodecahedral units. From this plot, we conclude that the substitution of S by I is more feasible in x = 2 – 4 region and the NW in this region is expected to be observed by experiment. We also understand the growth direction of Mo₄S₆ clusters by comparing CE and FE of 1-D and 2-D assemblies (refer Figure S4, Supplementary Information). Our calculations show that for pristine case, the 2-D assembly is energetically more favored than 1-D NW, however, all iodine doped 2-D systems become less stable as compared to respective 1-D NWs, due to its geometrical constraint in increasing the number of Mo-Mo bonds. Overall, it is concluded that this cluster is preferred to grow linearly without the help of any substrate.

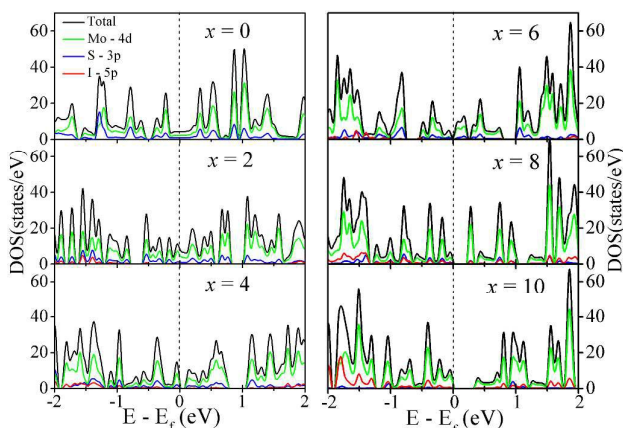


Figure 4. DOS of $\text{Mo}_8\text{S}_{12-x}\text{I}_x$ NWs and corresponding x values are marked in the respective panels.

Since the local structures of $\text{Mo}_8\text{S}_{12-x}\text{I}_x$ NWs are changing with respect to I atom concentration, it is also expected to reflect on its mechanical properties.

The Young's modulus (Y), is calculated from,

$$Y = \frac{k \cdot c}{A} \quad (3)$$

where ' A ' is the cross sectional area of the NW, obtained from $\pi \times d^2 / 4$, in which ' d ' is the sum of center-to-center distance between farthest atoms on the cross sectional plane of the wire and the covalent radii of the corresponding atoms, ' k ' is the force constant that is deduced from second derivative of plot of total energy (E) vs lattice constant and ' c ' is equilibrium lattice constant of the NW. The calculated Y values of the NWs are given in Table 1. The pristine NW has the highest Y value of 133 GPa owing to the covalent nature of Mo-S bonds. For the NW with $x = 2$, covalency is decreased, in addition of distortion of the core tetrahedral structure, which together decrease the Y value to 98.9 GPa. Similarly, more distortion in the structure of tetrahedral network, the Y value of NW with $x = 4$ reduces further to 87.4 GPa. Surprisingly for $\text{Mo}_8\text{S}_6\text{I}_6$ NW, the Y value increases to 98 GPa. This reversal in the trend is due to the significant change in the backbone structure of the NW to Mo_6 octahedron, where the strength of Mo-Mo bonds overshadow the effect of ionic Mo-I bonds. However, for $x > 6$, the Y value decreases slowly with increasing x . Finally, for $x = 12$, there is a huge fall in the value of Y which is observed to be 41.3 GPa, due to weakly interacting Mo_8 dodecahedral clusters. It is worthy to discuss that $\text{Mo}_6\text{S}_9-x\text{I}_x$ NWs are always higher Y values as compared to respective $\text{Mo}_8\text{S}_{12-x}\text{I}_x$ NWs as former type of NW has almost uniform dimension along its axis.

Next, the deduced density of states (DOS) of all $\text{Mo}_8\text{S}_{12-x}\text{I}_x$ NWs are shown in Figure 4. It is clear from the DOS of pure Mo_8S_{12} NW that it is metallic in nature with strong hybridization between Mo and S states lying between -1.5 to -0.5 eV. Moreover, electronic states are well spread across the Fermi level (E_f), which imparts good electronic conductivity to this NW. In contrast, the Mo_6S_9 NW is semiconducting nature with well localized electronic states around E_f ³². Similar to pristine

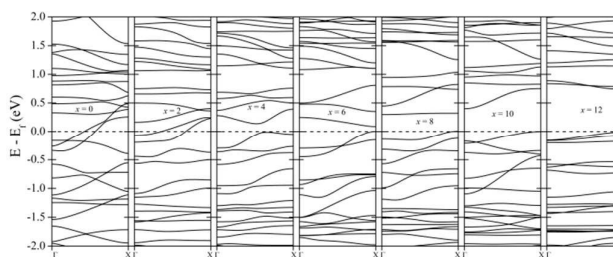


Figure 5. Band structure of $\text{Mo}_8\text{S}_{12-x}\text{I}_x$ NWs and the corresponding x values are written in the top panel.

NW, metallic character is observed in $\text{Mo}_8\text{S}_{10}\text{I}_2$ NW. Upon further doping, NWs with $x = 4$ and 6 become semiconducting in nature with band gaps (E_g) of 0.15 and 0.08 eV, respectively.

As the result of locally increasing Mo-Mo interaction in these NWs, semiconducting nature is observed from our work.

In order to get more details about the feature of valence band (VB) and conduction band (CB) of $\text{Mo}_8\text{S}_{12-x}\text{I}_x$ NWs, the band structures are plotted and reported in Figure 5. It is observed from this figure that the pristine NW has comparatively well dispersed VB than the other NWs and two states are crossing the E_f . While for $\text{Mo}_6\text{S}_{10}\text{I}_2$ NW, the VB is less dispersed that infers the lowering of electron mobility in this NW. Notably, the NWs with $x = 4, 6, 8$ and 10 are semiconductors with the E_g values of 0.15, 0.08, 0.29, and 0.40 eV, respectively. Overall, the E_g of NWs increases with x . Thus, we conclude that the electronic properties of the $\text{Mo}_8\text{S}_{12-x}\text{I}_x$ NWs are tunable *via* I atom doping.

Conclusions

From our study, we propose a new atomic structure for Mo_6S_9 NW obtained by condensing Mo_4S_6 clusters rather than Mo_6S_8 clusters as attempted earlier. The proposed structure of $\text{Mo}_8\text{S}_{12-x}\text{I}_x$ NW is found to be more stable in pristine form. However, Iodine doping reduces its stability significantly as compared to NW having Mo_6 octahedra as building block. Interestingly, the local structure of proposed NW is strongly influenced by I atom doping which in turn affects its mechanical and electronic properties, mainly due to the variations in Mo-Mo bonding. Further, we deduced electronic properties of the pristine NW and found them to be metallic in nature with well dispersed VB; whereas, the iodine doped NWs have semiconducting nature with narrowly dispersed VB and the E_g value increases with the dopant concentration.

Acknowledgements

All the authors acknowledge DST-India for its financial support through Fast Track scheme. We acknowledge Prof. Vijay Kumar for fruitful discussions. JK acknowledges CSIR-India for providing a Senior Research Fellowship. We also thank CDAC, CSIR-CECRI, CMMACS, and NCL for sharing their high performance computing facilities.

Notes and references

- 1 F. Schwierz, J. Pezoldt and R. Granzner, *Nanoscale*, 2015, **7**, 8261-8283.
- 2 H. Wang, F. Liu, W. Fu, Z. Fang, W. Zhou and Z. Liu, *Nanoscale*, 2014, **6**, 12250-12272.
- 3 I. Song, C. Park and H. C. Choi, *RSC Advances*, 2015, **5**, 7495-7514.
- 4 J. Karthikeyan, V. Kumar and P. Murugan, *Physical Chemistry Chemical Physics*, 2013, **15**, 13077-13082.
- 5 J. Pu, L.-J. Li and T. Takenobu, *Physical Chemistry Chemical Physics*, 2014, **16**, 14996-15006.
- 6 Q. Peng and S. De, *Physical Chemistry Chemical Physics*, 2013, **15**, 19427-19437.
- 7 S. Bertolazzi, J. Brivio and A. Kis, *Acs Nano*, 2011, **5**, 9703-9709.
- 8 X. Zhong, W. Zhou, Y. Peng, Y. Zhou, F. Zhou, Y. Yin and D. Tang, *RSC Advances*, 2015, **5**, 45239-45248.
- 9 M. Buscema, J. O. Island, D. J. Groenendijk, S. I. Blanter, G. A. Steele, H. S. J. van der Zant and A. Castellanos-Gomez, *Chemical Society Reviews*, 2015, **44**, 3691-3718.
- 10 P. Papakonstantinou, M. McMullan, N. J. Sun, M. X. Li, W. Z. Zhou and D. Mihailovic, *Biosens. Bioelectron.*, 2011, **26**, 1853-1859.
- 11 A. Majkić, C. Gadermaier, N. Celic, P. Topolovsek, G. Bratina and D. Mihailovic, *Solar Energy Materials and Solar Cells*, 2014, **127**, 63-66.
- 12 X. Hu, W. Zhang, X. Liu, Y. Mei and Y. Huang, *Chemical Society Reviews*, 2015, **44**, 2376-2404.
- 13 H. Yu, C. Zhu, K. Zhang, Y. Chen, C. Li, P. Gao, P. Yang and Q. Ouyang, *Journal of Materials Chemistry A*, 2014, **2**, 4551-4557.
- 14 F. Thole, L. F. Wan and D. Prendergast, *Physical Chemistry Chemical Physics*, 2015, **17**, 22548-22551.
- 15 K. F. Mak, C. Lee, J. Hone, J. Shan and T. F. Heinz, *Phys Rev Lett*, 2010, **105**.
- 16 C. Mai, A. Barrette, Y. F. Yu, Y. G. Semenov, K. W. Kim, L. Y. Cao and K. Gundogdu, *Nano Lett*, 2014, **14**, 202-206.
- 17 C. Mai, Y. G. Semenov, A. Barrette, Y. F. Yu, Z. H. Jin, L. Y. Cao, K. W. Kim and K. Gundogdu, *Phys Rev B*, 2014, **90**.
- 18 S. Gemming, G. Seifert and I. Vilfan, *Phys Status Solidi B*, 2006, **243**, 3320-3324.
- 19 J. Karthikeyan, V. Kumar and P. Murugan, *J Phys Chem C*, 2015, **119**, 13979-13985.
- 20 P. Murugan, V. Kumar, Y. Kawazoe and N. Ota, *Nano Lett*, 2007, **7**, 2214-2219.
- 21 J. Kibsgaard, A. Tuxen, M. Levisen, E. Laegsgaard, S. Gemming, G. Seifert, J. V. Lauritsen and F. Besenbacher, *Nano Lett*, 2008, **8**, 3928-3931.
- 22 A. Meden, A. Kodre, J. P. Gomilsek, I. Arcon, I. Vilfan, D. Vrbanic, A. Mrzel and D. Mihailovic, *Nanotechnology*, 2005, **16**, 1578-1583.
- 23 M. McMullan, N. Sun, P. Papakonstantinou, M. Li, W. Zhou and D. Mihailovic, *Biosensors and Bioelectronics*, 2011, **26**, 1853-1859.
- 24 N. Sun, M. McMullan, P. Papakonstantinou, H. Gao, X. X. Zhang, D. Mihailovic and M. X. Li, *Anal. Chem.*, 2008, **80**, 3593-3597.
- 25 H. Lin, H. M. Cheng, X. P. Miao, P. Papakonstantinou, D. Mihailovi and M. X. Li, *Electroanalysis (N. Y.)*, 2010, **21**, 2602-2606.
- 26 T. Yang, S. Berber and D. Tomanek, *Phys Rev B*, 2008, **77**.
- 27 F. Demiray and S. Berber, *J Phys Chem C*, 2012, **116**, 23833-23837.
- 28 I. Popov, S. Gemming, S. Okano, N. Ranjan and G. Seifert, *Nano Lett*, 2008, **8**, 4093-4097.
- 29 J. Buh, A. Kovic, A. Mrzel, Z. Jaglicic, A. Jesih and D. Mihailovic, *Nanotechnology*, 2014, **25**.
- 30 S. H. Wen, Z. F. Hou and K. L. Han, *J Phys Chem C*, 2009, **113**, 18436-18440.
- 31 R. Tenne and M. Redlich, *Chemical Society Reviews*, 2010, **39**, 1423-1434.
- 32 A. B. Laursen, S. Kegnaes, S. Dahl and I. Chorkendorff, *Energy & Environmental Science*, 2012, **5**, 5577-5591.
- 33 Y. G. Li, H. L. Wang, L. M. Xie, Y. Y. Liang, G. S. Hong and H. J. Dai, *J Am Chem Soc*, 2011, **133**, 7296-7299.
- 34 G. Seifert, J. Tamuliene and S. Gemming, *Comp Mater Sci*, 2006, **35**, 316-320.
- 35 S. Gemming, J. Tamuliene, G. Seifert, N. Bertram, Y. D. Kim and G. Gantefor, *Appl Phys a-Mater*, 2006, **82**, 161-166.
- 36 P. Murugan, V. Kumar, Y. Kawazoe and N. Ota, *J Phys Chem A*, 2007, **111**, 2778-2782.
- 37 G. Paglia, E. S. Bozin, D. Vengust, D. Mihailovic and S. J. L. Billinge, *Chem Mater*, 2006, **18**, 100-106.
- 38 J. Zhou, J. Zhou, N. Camillone and M. G. White, *Physical Chemistry Chemical Physics*, 2012, **14**, 8105-8110.
- 39 S. Gemming and G. Seifert, *Appl Phys a-Mater*, 2006, **82**, 175-179.
- 40 J. M. Lightstone, M. J. Patterson, P. Liu, J. C. Lofaro and M. G. White, *J Phys Chem C*, 2008, **112**, 11495-11506.
- 41 G. Kresse and D. Joubert, *Phys Rev B*, 1999, **59**, 1758-1775.
- 42 P. E. Blochl, *Phys Rev B*, 1994, **50**, 17953-17979.
- 43 J. P. Perdew, J. A. Chevary, S. H. Vosko, K. A. Jackson, M. R. Pederson, D. J. Singh and C. Fiolhais, *Phys Rev B*, 1992, **46**, 6671-6687.